Article

Genesis and effects of swapping bi-layers in hexagonal GeSb2Te4

Jiang-Jing Wang, Jun Wang, Hongchu Du, Lu Lu, Peter C. Schmitz, Johannes Reindl, Antonio M. Mio, Chun-Lin Jia, Evan Ma, Riccardo Mazzarello, Matthias Wuttig, and Wei Zhang

Chem. Mater., **Just Accepted Manuscript** • DOI: 10.1021/acs.chemmater.8b01900 • Publication Date (Web): 02 Jul 2018

Genesis and effects of swapping bi-layers in hexagonal $GeSb_2Te_4$

Jiang-Jing Wang[1,‡], Jun Wang[1,‡], Hongchu Du[2], Lu Lu[3], Peter C. Schmitz[4], Johannes Reindl[5], Antonio M. Mio[5], Chun-Lin Jia[2,3], Evan Ma[1, 6], Riccardo Mazzarello[4], Matthias Wuttig[5,7], Wei Zhang*[,1]

[1] Center for Advancing Materials Performance from the Nanoscale, State Key Laboratory for Mechanical Behavior of Materials, Xi'an Jiaotong University, Xi'an 710049, China

[2] Peter Grünberg Institute and Ernst Ruska-Centre for Microscopy and Spectroscopy with Electrons, Forschungszentrum Jülich GmbH, 52425 Jülich, Germany

[3]The School of Electronic and Information Engineering, State Key Laboratory for Mechanical Behavior of Materials, Xi'an Jiaotong University, Xi'an 710049, China

[4] Institute for Theoretical Solid-State Physics, JARA-FIT and JARA-HPC, RWTH Aachen University, 52074 Aachen, Germany

[5] Institute of Physics IA, JARA-FIT and JARA-HPC, RWTH Aachen University, 52074 Aachen, Germany

[6] Department of Materials Science and Engineering, Johns Hopkins University, Baltimore, MD 21218, USA

[7] Peter Grünberg Institute (PGI 10), Forschungszentrum Jülich GmbH, 52425 Jülich, Germany

ABSTRACT: Disorder plays an essential role in shaping the transport properties of GeSbTe phase-change materials (PCMs) to enable non-volatile memory technology. Recently, increasing efforts have been undertaken to investigate disorder in the stable hexagonal phase of GeSbTe compounds, focusing on a special type of swapping bi-layer defects. This configuration has been claimed to be the key element for a new mechanism for phase-change memory. Here, we report a direct atomic-scale chemical identification of these swapping bi-layer defects in hexagonal $GeSb_2Te_4$ together with nanoscale atomic modelling and simulations. We identify the intermixing of Sb and Te in the bi-layer to be the essential ingredient for the stability of the defects, and elucidate their abundance as due to the small energy cost. The bi-layer defects are demonstrated to be ineffective in altering the electron localization nature that is relevant to transport properties of hexagonal $GeSb_2Te_4$. Our work paves the way for future studies of layer-switching dynamics in GeSbTe at the atomic and electronic level, which could be important to understand the new switching mechanism relevant to interfacial phase-change memory.

Phase-change materials (PCMs) are one of the most promising candidates for non-volatile electronic memory technology,[1-7] which could achieve substantial improvements in computing performance of electronic devices.[8] The basic principle of phase-change memory is the exploitation of the capability of PCMs to undergo fast and reversible transitions between the amorphous and crystalline state, resulting in a large change in electrical resistance between the two states.[1] Among the explored PCMs, GeSbTe compounds along the $GeTe$-Sb_2Te_3 pseudo-binary line, such as $Ge_2Sb_2Te_5$ and $GeSb_2Te_4$, are the most widely used and studied PCMs.[9-12] Upon fast crystallization, GeSbTe compounds form a cubic rocksalt phase, in which Te atoms take one sublattice, while Ge and Sb atoms as well as atomic vacancies occupy the other.[13, 14] This crystalline phase is rather unconventional, as it accommodates a very large amount of atomic vacancies, e.g. 12.5% in $GeSb_2Te_4$, which is orders of magnitude higher as compared to other semiconductors.[15] These atomic vacancies are randomly arranged on the cation-like sublattice of GeSbTe, leading to a strong localization of electronic wave-functions near the Fermi level, and thereby a disorder-induced insulating phase.[16-21] Further thermal annealing at elevated temperatures triggers extensive vacancy diffusion on the cation-like sublattice, driving the randomly distributed atomic vacancies to form ordered planes.[11] Such a vacancy ordering process induces a structural transition from cubic rocksalt to hexagonal stacking as well as an electronic transition from insulating to metallic.[16, 17] Similar disorder-driven phenomena were also observed in the closely related compounds $SnSb_2Te_4$ and $SnBi_2Te_4$.[22]

The ordered hexagonal phase of GeSbTe compounds, consisting of alternating Ge/Sb and Te atomic layers and gaps, is regarded as the stable phase,[11, 13] yet a non-negligible amount of disorder and defects is observed in hexagonal samples, including stacking faults and Ge/Sb intermixing, as revealed by recent transmission electron microscopy experiments.[23-27] These defects were consistently found in all layer-structured GeSbTe samples produced by various deposition and epitaxy methods, [23-30] and some of them were proposed to be essential to the switching mechanisms[23, 30] in interfacial phase-change memory devices (iPCM).[31] In this novel family of devices, phase transitions were claimed to take place between two crystalline states, [31-33] leading to reduced power consumption and faster switching speeds as compared to conventional phase-change memory. However, the underlying reasons why these defects can form and their effects on the electronic and transport properties still remain unclear. To shed light on

these issues, it is necessary to carry out thorough structural and chemical characterizations as well as large-scale materials modeling and simulations.

In this work, we focus on the hexagonal phase of $GeSb_2Te_4$ (abbreviated as hex-GST in the following), since its transport properties have been well investigated.[16, 34] In line with the previous work,[16] the samples were prepared by magnetron sputtering and were annealed at 300 °C for half an hour (see Methods for detail information). The measured X-ray diffraction (XRD) pattern confirms the samples to be in the hexagonal phase (**Figure S1**). The unit cell of the ideal hex-GST consists of three septuple-layer atomic blocks with the first atomic layer being indexed by "a", "b" and "c", which represent the in-plane atomic positions (0, 0), (2/3, 1/3) and (1/3, 2/3) in each layer (**Figure 1a**). The whole stacking sequence is –*g*-abcabca-*g*-bcabcab-*g*-cabcabc–, where *g* represents the gaps between the structural blocks. The gaps are commonly referred as "van der Waals gaps", while it has been shown recently that additional weak covalent-like interactions are present in addition to van der Waals forces.[35, 36] The chemical distribution inside an ideal septuple-layer block is –Te-Sb-Te-Ge-Te-Sb-Te–, as indicated by the yellow, green and red spheres in **Figure 1a**. However, the microstructure in real materials is far more complex due to the existence of various defects, as discussed in the following.

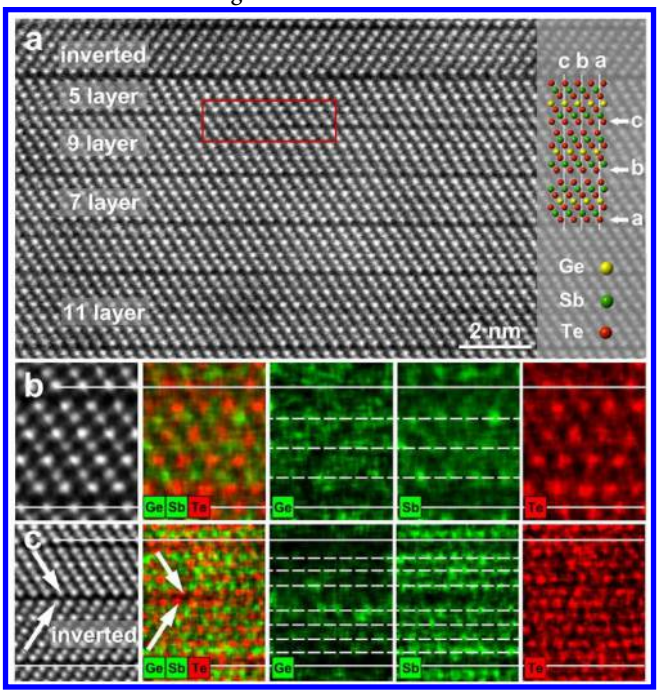

Figure 1. Structural and chemical characterizations of hex-GST. **a** A typical HAADF image of the hexagonal $GeSb_2Te_4$ sample. The ideal model is shown on the right side, but the microstructure in real materials is far more complex. One swapping bi-layer defect is marked by the red box. **b** and **c** show the HAADF images and the corresponding overlaid and elemental EDX mappings of a septuple-layer block, and a septuple-layer block in contact with an inverted nonuple-layer block. EDX mappings unambiguously pin down the chemistry of the layer-structured $GeSb_2Te_4$ and $Ge_2Sb_2Te_5$ blocks, i.e. the Ge/Sb intermixing appear on cation-like layers, and the Te layers separate the cation-like layers and terminate the structural blocks.

We carried out spherical aberration corrected (Cs-corrected) high angle annular dark field (HAADF) scanning transmission electron microscopy (STEM) and the energy-dispersive X-ray mapping (EDX) experiments to investigate the atomic structure and chemistry of hex-GST (see Methods for detail information). The intensity peaks (bright spots) in HAADF images appear at the positions of atomic columns, and the intensity of the peaks is approximately proportional to the square of the averaged atomic number Z of each column along the view direction.[37] Ge (Z=32) shows much lower image intensity than Sb (Z=51) and Te (Z=52). It is not feasible to distinguish Sb and Te from HAADF image owing to their very close atomic number. However, with EDX mapping, the elemental distribution can be unambiguously determined.[14] From previous XRD[13] and STEM[25, 26] experiments as well as density functional theory (DFT) simulations,[38] it is derived that a) the septuple-layer $GeSb_2Te_4$ blocks are terminated by Te layers, and b) the cation-like layers are occupied by both Ge and Sb. Our STEM-EDX experiments provide direct proof for these two structural features. **Figure 1b** shows the HAADF image, and the corresponding overlaid and elemental EDX mappings. Clearly, Ge/Sb compositional disorder is found on the cation-like layers (marked with dashed lines), and the three cation-like layers are sandwiched by four anion-like Te layers.

It can be seen from the topside of **Figure 1a** that the internal stacking sequence of septuple-layer blocks can be inverted, i.e. atomic layers can be arranged as "acb" instead of "abc", producing a twin-like structure from two adjacent blocks. Such defects appear everywhere in the samples and apparently do not show long range order, i.e. a regular arrangement. The size of these defects varies from one to several tens of structural blocks (**Figure S2**). **Figure 1c** shows the HAADF image and the corresponding EDX mapping of atomic blocks with inverted stacking. No visible difference in distribution of Ge and Sb atoms can be observed in the inverted atomic blocks. Hence, the formation of these defects does not require a local change of composition and the corresponding long range diffusion.

Many stacking faults, including quintuple-, nonuple- and even hendecuple-layer blocks, can be found in the HAADF image and EDX mapping in **Figure 1a** and **1c**. By evaluating the image intensity, they are identified as Sb_2Te_3, $Ge_2Sb_2Te_5$ and $Ge_3Sb_2Te_6$ blocks, respectively (**Figure S3**). However, if we examine the structural details on a large length scale, the stacking faults are actually found to be connected via a special type of bi-layer defects (**Figure 1a** red box). These swapping bi-layer defects are proposed to be the key element to enable layer-switching in layered GeSbTe for iPCM devices,[23, 30] as a clear reconfiguration of atomic blocks and gaps was observed under extensive exposure to the focused electron beam in TEM.[23] It is noted that such local structural rearrangement is mainly caused by the very high kinetic energy brought by the very well focused electron beam on an area of several tens of picometers. No visible structural changes can be observed in standard STEM experiments using unfocused electron beam with a recording time of just a few minutes, see **Figure S4**. The presence of the bi-layer defects is abundant, and the planar defect density is estimated to be one per ~75 nm^2, as counted in a few hundreds of HAADF scans over several tens of grains. One such large-scale HAADF scan is shown in **Figure S5**.

However, until now, the chemistry of these swapping bi-layer defects has remained unclear, as the two layers show similar contrast in the HAADF images. This issue can be properly resolved by EDX mapping experiments. The HAADF image and the corresponding EDX mapping of a bi-layer defect is shown in **Figure 2**. Since the Ge signals are too weak to capture, the signals of Ge and Sb were collected together, for the sake of technical convenience. Since the HAADF image intensities of the two layers are similar, and one of them has strong Te signals, we can derive that the other layer is mostly occupied by Sb. A clear crossing of the Sb-rich and Te-rich layer is observed, and the swapping path is shown to be continuous and smooth. The overlaid EDX mapping (**Figure 2d**) also indicates some intermixing of Sb and Te in the bi-layers.

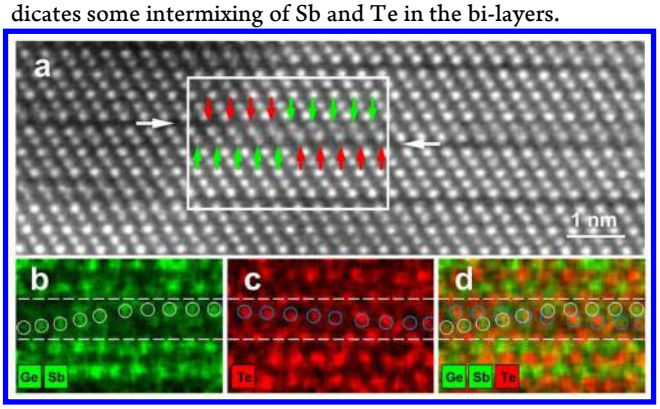

Figure 2. The HAADF image and the corresponding EDX mapping of a bi-layer defect. a The HAADF image of bilayer defect. Green and red arrows mark the Sb-rich and Te-rich layer, respectively. **b-d** The corresponding EDX mappings of the area inside the white box marked in **a**. The centers of each Ge/Sb and Te atomic column are marked with white and blue cycles, respectively. A smooth and continuous crossing of the Sb-rich and Te-rich layer is observed. The overlaid EDX mapping in **d** also indicates some intermixing of Sb and Te in the bi-layers, which is identified as the essential ingredient for the stability of the defects from DFT simulations.

Next, we turn to DFT calculations to gain further understanding of the bi-layer defects. All the DFT calculations presented in the following were done by using the CP2K package[39] (see Methods for detail information). To address the stability and the effects of the bi-layer defects, large-scale materials modeling is needed, as the typical length of the bi-layer defects is ~3 nm (**Figure 1a** and **Figure 2a**). To this end, a large orthorhombic supercell with the size of 9.6 × 1.3 × 4.1 nm^3 (containing 1,638 atoms) was constructed. In order to keep the periodic condition for DFT calculations, two bi-layer defects with opposite directions were considered. This model corresponds to a reasonable planar density of bi-layer defects of about one per 20 nm^2, and it is not feasible computationally to investigate larger models corresponding to the experimental value. The model was subsequently relaxed using DFT, and the bi-layer defects were shown to be robust (**Figure 3a** and **Figure S6**). The key ingredient to preserve the "shape" of the bi-layer defects stable against strong atomic relaxation is the intermixing of Sb and Te in these two layers. For the model with pure Sb and Te layers, the size of the bi-layer defect shrinks drastically upon relaxation, ending up with a sharp jump of Sb-Sb or Te-Te contacts, similar to the small-scale models built in Refs. [30, 40] (**Figure S6a**). The Sb-Te intermixing could also explain the blurriness of the HAADF image of bi-layer defects (**Figure 2a**), i.e. the additional distortion brought by Sb-Te intermixing disorder leads to deviations from the atomic centers. We quantify this Sb-Te intermixing disorder by counting the fraction of Sb-Te, Sb-Sb and Te-Te bonds in the bi-layer, which shows a broad distribution of bonds from 2.8 to 3.3 Å in the intermixed model but very sharp distributions in the non-mixed model (**Figure S6c-d**). A thorough comparison between the STEM-EDX experiments and DFT simulations confirms the validity of the bi-layer defects model we built, making the subsequent analyses of energetics, electronic and transport properties reliable.

It is important to note that the energy cost of the bi-layer defects is only about 9.8 meV/atom with respect to the ideal hex-GST model (**Figure 4a**), which is relatively small as compared to the energy difference between the ideal hexagonal phase and the metastable rocksalt phase ~70 meV/atom.[17] It is noted that such value is meaningful only if the density of these bi-layer defects is comparable to or larger than that found in experiments. In our model, the planar density is one bilayer per ~20 nm^2, which is more than three times higher than the experimental value, one bilayer per ~75 nm^2. The energy cost per atom of the defect will be further reduced, if larger standard $GeSb_2Te_4$ blocks are added to the model. Such small energy cost explains why massive bi-layer defects can be present in hex-GST. Note that the metastable rocksalt phase is thermally stable at room temperature for decades. This also holds for the bi-layer defects found in the hexagonal phase. Due to the high thermal stability of these defects, it is important to investigate their effects on the electronic and transport properties of hex-GST.

We calculated the density of states (DOS) for both the bi-layer defects model and the ideal model (**Figure 3b** and **Figure 4a**). Although the size of the band gap is reduced due to the presence of bi-layer defects, the transport properties, in particular at room and low temperatures, are mainly determined by the nature of the electronic states at the top of the valence band. This is due to the spontaneous formation of vacancies in the cation-like layers (so called self-doping),[41] which shifts the Fermi level to the edge of the valence band and results in *p*-type behavior.[16] The inverse participation ratio (IPR) is a direct measure of the degree of localization of the electronic states[17] (see Methods for detail information). For GeSbTe models containing a few thousands of atoms, 0.005 is a reasonable threshold value to distinguish localized states from extended ones.[17, 18] Clearly, the IPR values at the top of the valence band are far below this value for both the defective and ideal model, indicative for delocalized states. Moreover, the charge-density plots of the electronic wave-functions (marked with blue surfaces) of the highest occupied molecular orbital (HOMO) states of the two models show delocalized behaviour (**Figure 3c** and **Figure 4a**). On the other hand, the effects of the bi-layer defects on the unoccupied states are more pronounced, resulting in multiple localized states at the tail of the conduction band (**Figure 3b**). This may stem from the fact that the unfavorable Sb-Te intermixing raises the total energy of the system as well as the local electron density, creating multiple high energy bands in the tail of the conduction band, in line with the electronic structure of rocksalt GST with Sb-Te antisite pairs.[42] Indeed, the wavefunctions of these empty

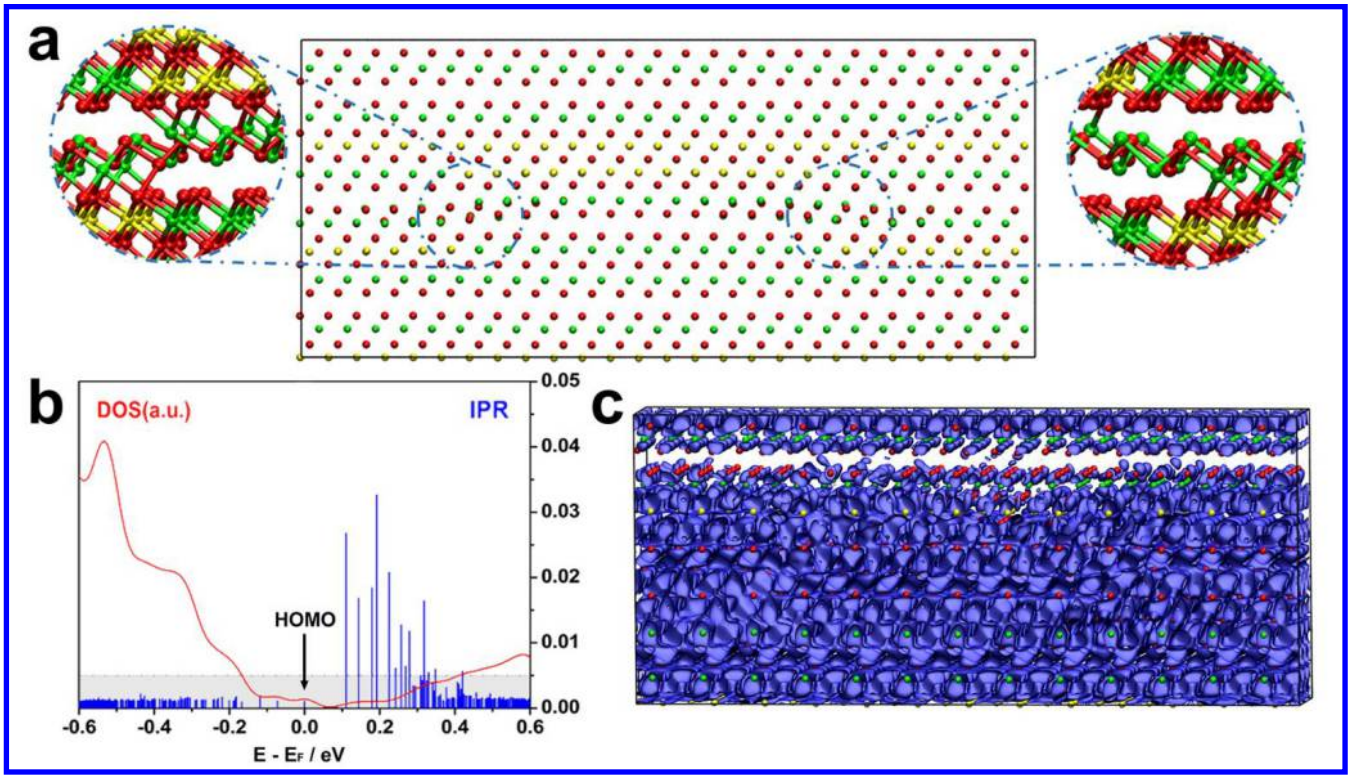

Figure 3. DFT modelling of the bi-layer defects. a Two stable bi-layers are found in the relaxed hex-GST model. The energy cost is quite low, ~9.8 meV/atom. **b-c** The calculated density of state (DOS) and inverse participation ratio (IPR) and the highest occupied molecular orbital (HOMO) state of the relaxed model shown in **a**. The empirical threshold IPR value 0.005 that distinguishes localization from delocalization is marked in grey. The IPR values at the top of the valence band in **b** are far below the empirical threshold value, distinguishing localized states from extended ones. The distribution of electronic wave functions of the HOMO state (blue isosourfaces rendered with an isovalue of 0.001 a.u.) shows a clear extended nature, explaining the metallic character measured in hex-GST samples, as the Fermi level is pinned at the top of valence band due to self-doping effects. A couple of localized states at the tail of the conduction band are created by the bi-layer defects (**Figure S7**), which may strongly affect the transport properties at elevated temperatures, where massive electron excitations take place.

localized states are found around the swapping fronts of these bi-layer defects (**Figure S7**). Yet, these electronic states would only be thermally populated at elevated temperatures well above room temperature. At room tempera-ture and below, only states in the valence band are utilized for transport, which have been shown above to be delocalized. Hence, the simulated electronic and localization properties are well in line with the transport measurements, where the hex-GST samples annealed at 300 °C display metallic behavior at low temperatures.[16]

We performed similar analyses for other defects observed in **Figure 1**. Three 9×9×1 hexagonal supercells with size 3.8×3.8×4.1 nm^3 were constructed to include an inverted septuple-layer block, a stacking fault due to a pair of quintuple-layer and nonuple-layer, and the Ge/Sb compositional disorder on cation-like layers. The corresponding sketch of atomic structure, DOS, IPR and HOMO state are presented in **Figure 4 b-d**. The energy costs of the three defective models are quite small, 1.0, 4.5 and 6.8 meV/atom, respectively, explaining their massive presence in the experimental samples. Electron localization is not found in any of these models, neither in the valence band nor the conduction band. It is technically not yet feasible to consider spin-orbit coupling effects in these large-scale models, but nevertheless, we have shown that they do not lead to any qualitative change in electron localization properties in small-scale GeSbTe models.[18] All the above DFT simulations were done at zero temperature, in which the entropy effects were not included. It is noted that entropy could also play some role in stabilizing these defects, in particular, during the dynamical forming process at elevated temperatures (the hexagonal samples were obtained at 300 °C in this work). But if their energy cost is too high, these defects will vanish upon cooling. Nevertheless, our DFT simulations should reflect the properties of hex-GST at room temperature that are relevant to memory applications, as information is read at room temperature.

In summary, we pin down the structural and chemical features of the major defects observed in hex-GST through chemi-STEM experiments. DFT calculations attribute their abundance to the low energy cost of defect formation. The calculated electronic structure shows that the metallic character of the compound is not strongly affected by stacking faults, twin-like structures as well as Ge/Sb compositional disorder. The presence of the bi-layer defects does not result in electron localization in the valence band, but can create several localized states at the tail of the conduction band. This will not affect the metallic behavior at room and low temperatures as the Fermi level lies at the top of the valence band, but may play some role in shaping the transport properties at elevated temperatures or under other strong external stimuli, where

massive electron excitations to the conduction band take place. All these defects may act as possible sources for electron scattering, affecting the quantitative value of electrical resistance in hex-GST,[16, 25] but cannot lead to any qualitative change in transport character.

Further investigations are required to elucidate the dynamics of the swapping bi-layer defects in hex-GST, e.g. how they develop from the rocksalt phase and how they change under external stimuli. It is noted that, even in the presence of a massive number of defects, hex-GST still has very low resistance value. As far as iPCMs are concerned, it turns out that the high resistance state has a resistance comparable to that of the amorphous phase of GeSbTe.[31] It is thus essential to experimentally pin down the structure and chemistry of this state. If it is crystalline, it is then very important to understand its transport properties, including the position of the Fermi level, carrier concentration and type. Our work paves the way for future structural and transport experiments, as well as for DFT-based molecular dynamics simulations to access the switching mechanisms in iPCM superlattices at the atomic and electronic level.

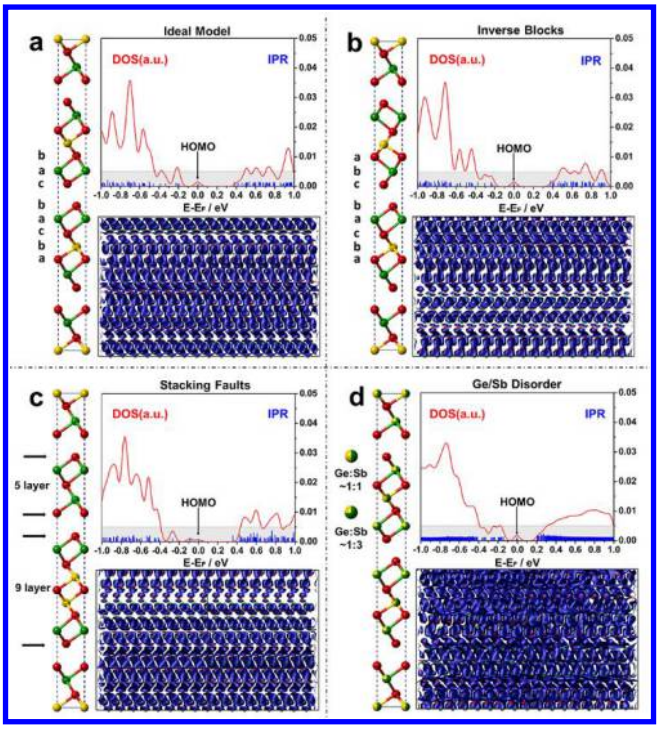

Figure 4. DFT modelling of ideal hex-GST and three types of defects. a-d show the sketch of the atomic structure, DOS and IPR and HOMO state of the ideal model, and the models containing an inverted septuple-layer block, a pair of quintuple-layer and nonuple-layer stacking fault, and the Ge/Sb compositional disorder on cation-like layers, respectively. The empirical threshold IPR value 0.005 that distinguishes localization from delocalization is marked in grey. The Ge:Sb ratio is fixed as ~1:1 for the center cation-like layer, and ~1:3 for the outer two cation-like layers. The isosurfaces of the four HOMO states all render a value of 0.001 a.u. Electron localization is not found in any of these models, neither in the valence band nor the conduction band.

At last, we note that the study of disorder in layer-structured ternary IV-V-chalcogenides and binary V-chalcogenides, including $GeSb_2Te_4$, $SnBi_2Te_4$, Sb_2Te_3, Bi_2Te_3 and many others, is not only important for the phase-change properties, but also for the topological insulating[43-45] as well as thermoelectric properties[46-48] of these solids. Similar bi-layer defects can even be found in Bi_2Te_3, but their effects to topological insulating and thermoelectric properties have not been taken into account yet.[49] Our work on structural and electronic characterizations of atomic disorder in layer-structured Ge-Sb-Te compounds hence can stimulate further investigations in this important and exciting direction.

METHODS

Sample preparation: The ~450 nm $GeSb_2Te_4$ thin films were deposited with the magnetron sputtering technique on Si (111) substrate. The samples were annealed in argon atmosphere (flow rate of 200 sccm) in a regular tube furnace with a 3 cm diameter quartz tube. The annealing temperature was raised to 300 °C from room temperature with a heating rate of 5 K/min. Then the samples were further annealed at 300 °C for 30 minutes. After the annealing process, the samples were cooled down to room temperature, and then were taken out from the furnace. The structure of annealed $GeSb_2Te_4$ films was checked by X-ray diffraction (XRD) on a Philips X'pert Materials Research Diffractometer (MRD).

TEM measurement: Cross-section TEM specimens were prepared by a Helios NanoLab 400S focused ion beam (FIB) system with a Ga ion beam at 30 kV beam energy and polished at 5 kV. The thinning and cleaning process were finished in a Fischione Nanomill with an Ar ion beam at energy of 900 eV for thinning and 500 eV for cleaning, the filament current was 0.21 mA and specimen tilt angles were ±10°. The thickness of TEM specimens is approximately 80nm. Aberration corrected high-angle annular dark-field scanning transmission electron microscopy (HAADF-STEM) and atomic energy dispersive X-ray (EDS) spectroscopy imaging were conducted at 200kV on an FEI Titan G2 80-200 Chemi-STEM microscope equipped with a high-brightness Schottky field emission electron gun, a probe Cs corrector and a Super-X EDX system.

DFT simulations: All simulations are carried out using the CP2K code[39]. In these simulations, Kohn-Sham orbitals are expanded in a Gaussian-type basis set of triple-zeta plus polarization quality, whereas the charge density is expanded in plane waves with the energy cutoff of 300 Ry and Γ point sampling in the Brillouin zone. Both the atomic positions and simulation cells of all the models presented in this work were fully relaxed by employing scalar-relativistic Goedecker pseudopotentials[50] and GGA-PBE functionals[51] with van der Waals corrections.[52]

Localization analysis: Cross-section TEM specimens were prepared by a H Inverse participation ratio (IPR) is used to characterize the degree of localization of a Kohn-Sham eigenstate a. In DFT calculations using CP2K, it is defined as $\mathbf{IPR} \equiv \sum_i |\Psi_{a,i}|^4 / (\sum_i |\Psi_{a,i}|^2)^2$ where $\Psi_{a,i}$ are the expansion coefficients of a with respect to the localized Gaussian-type orbitals (GTOs) forming the basis set (see above) and i runs over all the GTOs. For localized states, IPR is finite and provides an estimate for the inverse of the number of atoms on which the state is localized. On the contrary, for an extended state, IPR is equal to zero in infinitely large systems. Our DFT models are not infinite but contain more than 1000 atoms, therefore, the typical IPR value of extended states is around 0.001.

ASSOCIATED CONTENT

Supporting Information. Additional figures referenced in the text on the XRD analysis, HAADF images of various atomic blocks, electron beam exposure, intermixing disorder analysis and localization properties analysis. This material is available free of charge via the Internet at http://pubs.acs.org.

AUTHOR INFORMATION

Corresponding Author

* (W.Z.) Email: wzhang0@mail.xjtu.edu.cn

Author Contributions

‡These authors contributed equally.

ACKNOWLEDGMENT

J.-J. W. and J.W. contributed equally to this work. The authors thank Mrs. Doris Meertens and Mr. Maximilian Kruth for the TEM specimen preparation. W.Z. gratefully thanks the support of National Natural Science Foundation of China (61774123 and 51621063), the Youth Thousand Talents Program of China and the Young Talent Support Plan of Xi'an Jiaotong University, H.D., C.J., P.C.S., R.M. and M.W. acknowledge the funding by the DFG (German Science Foundation) within the collaborative research centre SFB 917 "Nanoswitches". E.M. acknowledges the support from the U.S. Department of Energy, Office of Science, Basic Energy Sciences, Division of Materials Sciences and Engineering, under Contract No. DE-FG02-13ER46056. The authors also acknowledge the computational resources provided by the HPCC platform of Xi'an Jiaotong University and JARA-HPC from RWTH Aachen University under project JARA0150. The authors also acknowledge the support by International Joint Laboratory for Micro/Nano Manufacturing and Measurement Technologies (IJL-MMMT) of Xi'an Jiaotong University. This work is also supported by the Science and Technology Department of Jiangsu Province under the grant agreement No. BK20170414. The research leading to these results received funding from the European Union Seventh Framework Programme (FP7/2007-2013) under Grant Agreement No. 340698.

REFERENCES

1. Wuttig, M.; Yamada, N., Phase-change materials for rewriteable data storage. *Nat. Mater.* **2007**, 6, 824-832.
2. Raoux, S.; Welnic, W.; Ielmini, D., Phase change materials and their application to nonvolatile memories. *Chem. Rev.* **2010**, 110, 240-267.
3. Wong, H.-S. P.; Raoux, S.; Kim, S. B.; Liang, J.; Reifenberg, J. P.; Rajendran, B.; Asheghi, M.; Goodson, K. E., Phase Change Memory. *Proc. IEEE* **2010**, 98, 2201-2227.
4. Xiong, F.; Liao, A. D.; Estrada, D.; Pop, E., Low-power switching of phase-change materials with carbon nanotube electrodes. *Science* **2011**, 332, 568-570.
5. Loke, D.; Lee, T. H.; Wang, W. J.; Shi, L. P.; Zhao, R.; Yeo, Y. C.; Chong, T. C.; Elliott, S. R., Breaking the speed limits of phase-change memory. *Science* **2012**, 336, 1566-1569.
6. Rao, F.; Ding, K.; Zhou, Y.-X.; Zheng, Y.; Xia, M.; Lv, S.; Song, Z.; Feng, S.; Ronneberger, I.; Mazzarello, R.; Zhang, W.; Ma, E., Reducing the stochasticity of crystal nucleation to enable subnanosecond memory writing. *Science* **2017**, 358, 1423-1427.
7. Burr, G. W.; Shelby, R. M.; Sidler, S.; Nolfo, C. d.; Jang, J.; Boybat, I.; Shenoy, R. S.; Narayanan, P.; Virwani, K.; Giacometti, E. U.; Kurdi, B. N.; Hwang, H., Experimental Demonstration and Tolerancing of a Large-Scale Neural Network (165 000 Synapses) Using Phase-Change Memory as the Synaptic Weight Element. *IEEE Trans. Electron Devices* **2015**, 62, 3498-3507.
8. Wong, H. S.; Salahuddin, S., Memory leads the way to better computing. *Nat. Nanotechnol.* **2015**, 10, 191-194.
9. Yamada, N.; Matsunaga, T., Structure of laser-crystallized Ge2Sb2+xTe5 sputtered thin films for use in optical memory. *J. Appl. Phys.* **2000**, 88, 7020-7028.
10. Kolobov, A. V.; Fons, P.; Frenkel, A. I.; Ankudinov, A. L.; Tominaga, J.; Uruga, T., Understanding the phase-change mechanism of rewritable optical media. *Nat. Mater.* **2004**, 3, 703-708.
11. Kooi, B. J.; De Hosson, J. T. M., Electron diffraction and high-resolution transmission electron microscopy of the high temperature crystal structures of GexSb2Te3+x (x=1,2,3) phase change material. *J. Appl. Phys.* **2002**, 92, 3584-3590.
12. Sun, Z.-M.; Zhou, J.; Ahuja, R., Structure of Phase Change Materials for Data Storage. *Phys. Rev. Lett.* **2006**, 96, 055507.
13. Matsunaga, T.; Yamada, N., Structural investigation of GeSb2Te4:A high-speed phase-change material. *Phys. Rev. B* **2004**, 69, 104111.
14. Zhang, B.; Zhang, W.; Shen, Z.-J.; Chen, Y.-J.; Li, J.-X.; Zhang, S.-B.; Zhang, Z.; Wuttig, M.; Mazzarello, R.; Ma, E.; Han, X.-D., Element-resolved atomic structure imaging of rocksalt Ge2Sb2Te5 phase-change material. *Appl. Phys. Lett.* **2016**, 108, 191902.
15. Wuttig, M.; Lusebrink, D.; Wamwangi, D.; Welnic, W.; Gillessen, M.; Dronskowski, R., The role of vacancies and local distortions in the design of new phase-change materials. *Nat. Mater.* **2007**, 6, 122-128.
16. Siegrist, T.; Jost, P.; Volker, H.; Woda, M.; Merkelbach, P.; Schlockermann, C.; Wuttig, M., Disorder-induced localization in crystalline phase-change materials. *Nat. Mater.* **2011**, 10, 202-208.
17. Zhang, W.; Thiess, A.; Zalden, P.; Zeller, R.; Dederichs, P. H.; Raty, J. Y.; Wuttig, M.; Blügel, S.; Mazzarello, R., Role of vacancies in metal-insulator transitions of crystalline phase-change materials. *Nat. Mater.* **2012**, 11, 952-956.
18. Zhang, W.; Wuttig, M.; Mazzarello, R., Effects of stoichiometry on the transport properties of crystalline phase-change materials. *Sci. Rep.* **2015**, 5, 13496.
19. Volker, H.; Jost, P.; Wuttig, M., Low-Temperature Transport in Crystalline Ge1Sb2Te4. *Adv. Funct. Mater.* **2015**, 25, 6390-6398.
20. Jost, P.; Volker, H.; Poitz, A.; Poltorak, C.; Zalden, P.; Schaefer, T.; Lange, F.; Schmidt, R. M.; Hollaender, B.; Wirtssohn, M. R.; Wuttig, M., Disorder-induced localization in crystalline pseudo-binary GeTe-Sb2Te3 alloys between Ge3Sb2Te6 and GeTe. *Adv. Funct. Mater.* **2015**, 25, 6399-6406.
21. Wang, J.-J.; Xu, Y.-Z.; Mazzarello, R.; Wuttig, M.; Zhang, W., A Review on Disorder-Driven Metal-Insulator Transition in Crystalline Vacancy-Rich GeSbTe Phase-Change Materials. *Materials* **2017**, 10, 862.
22. Schäfer, T.; Konze, P. M.; Huyeng, J. D.; Deringer, V. L.; Lesieur, T.; Müller, P.; Morgenstern, M.; Dronskowski, R.; Wuttig, M., Chemical Tuning of Carrier Type and Concentration in a Homologous Series of Crystalline Chalcogenides. *Chem. Mater.* **2017**, 29, 6749-6757.
23. Lotnyk, A.; Ross, U.; Dankwort, T.; Hilmi, I.; Kienle, L.; Rauschenbach, B., Atomic structure and dynamic reconfiguration of layered defects in van der Waals layered Ge-Sb-Te based materials. *Acta Mater.* **2017**, 141, 92-96.

24. Lotnyk, A.; Hilmi, I.; Ross, U.; Rauschenbach, B., Van der Waals interfacial bonding and intermixing in GeTe-Sb2Te3-based superlattices. *Nano Res.* **2018,** 11, 1676-1686.
25. Bragaglia, V.; Arciprete, F.; Zhang, W.; Mio, A. M.; Zallo, E.; Perumal, K.; Giussani, A.; Cecchi, S.; Boschker, J. E.; Riechert, H.; Privitera, S.; Rimini, E.; Mazzarello, R.; Calarco, R., Metal-Insulator Transition Driven by Vacancy Ordering in GeSbTe Phase Change Materials. *Sci. Rep.* **2016,** 6, 23843.
26. Hardtdegen, H.; Rieß, S.; Schuck, M.; Keller, K.; Jost, P.; Du, H.; Bornhöfft, M.; Schwedt, A.; Mussler, G.; Ahe, M. v. d.; Mayer, J.; Roth, G.; Grützmacher, D.; Mikulics, M., A model structure for interfacial phase change memories: Epitaxial trigonal Ge1Sb2Te4. *J. Alloys Compd.* **2016,** 679, 285-292.
27. Mio, A. M.; Privitera, S. M.; Bragaglia, V.; Arciprete, F.; Bongiorno, C.; Calarco, R.; Rimini, E., Chemical and structural arrangement of the trigonal phase in GeSbTe thin films. *Nanotechnology* **2017,** 28, 065706.
28. Momand, J.; Wang, R.; Boschker, J. E.; Verheijen, M. A.; Calarco, R.; Kooi, B. J., Interface formation of two- and three-dimensionally bonded materials in the case of GeTe-Sb2Te3 superlattices. *Nanoscale* **2015,** 7, 19136-19143.
29. Momand, J.; Wang, R.; Boschker, J. E.; Verheijen, M. A.; Calarco, R.; Kooi, B. J., Dynamic reconfiguration of van der Waals gaps within GeTe-Sb2Te3 based superlattices. *Nanoscale* **2017,** 9, 8774-8780.
30. Kolobov, A. V.; Fons, P.; Saito, Y.; Tominaga, J., Atomic Reconfiguration of van der Waals Gaps as the Key to Switching in GeTe/Sb2Te3 Superlattices. *ACS Omega* **2017,** 2, 6223-6232.
31. Simpson, R. E.; Fons, P.; Kolobov, A. V.; Fukaya, T.; Krbal, M.; Yagi, T.; Tominaga, J., Interfacial phase-change memory. *Nat. Nanotechnol.* **2011,** 6, 501-505.
32. Tominaga, J.; Kolobov, A. V.; Fons, P.; Nakano, T.; Murakami, S., Ferroelectric Order Control of the Dirac-Semimetal Phase in GeTe-Sb2Te3Superlattices. *Adv. Mater. Inter.* **2014,** 1, 1300027.
33. Küpers, M.; Konze, P. M.; Maintz, S.; Steinberg, S.; Mio, A. M.; Cojocaru-Miredin, O.; Zhu, M.; Müller, M.; Luysberg, M.; Mayer, J.; Wuttig, M.; Dronskowski, R., Unexpected Ge-Ge Contacts in the Two-Dimensional Ge4 Se3 Te Phase and Analysis of Their Chemical Cause with the Density of Energy (DOE) Function. *Angew. Chem. Int. Ed.* **2017,** 56, 10204-10208.
34. Breznay, N. P.; Volker, H.; Palevski, A.; Mazzarello, R.; Kapitulnik, A.; Wuttig, M., Weak antilocalization and disorder-enhanced electron interactions in annealed films of the phase-change compound GeSb2Te4. *Phys. Rev. B* **2012,** 86, 205302.
35. Wang, R.; Lange, F. R. L.; Cecchi, S.; Hanke, M.; Wuttig, M.; Calarco, R., 2D or Not 2D: Strain Tuning in Weakly Coupled Heterostructures. *Adv. Funct. Mater.* **2018,** 1705901.
36. Wang, J.; Ronneberger, I.; Zhou, L.; Lu, L.; Deringer, V. L.; Zhang, B.; Tian, L.; Du, H.; Jia, C.; Qian, X.; Wuttig, M.; Mazzarello, R.; Zhang, W., Unconventional two-dimensional germanium dichalcogenides. *Nanoscale* **2018,** 10, 7363-7368.
37. Pennycook, S. J.; Nellist, P. D., *Scanning Transmission Electron Microscopy Imaging and Analysis*. Springer-Verlag: New York, USA, 2002.
38. Da Silva, J.; Walsh, A.; Lee, H., Insights into the structure of the stable and metastable (GeTe)m(Sb2Te3)n compounds. *Phys. Rev. B* **2008,** 78, 224111.
39. Hutter, J.; Iannuzzi, M.; Schiffmann, F.; VandeVondele, J., cp2k:atomistic simulations of condensed matter systems. *WIREs Comput. Mol. Sci.* **2014,** 4, 15-25.
40. Yu, X.; Robertson, J., Atomic Layering, Intermixing and Switching Mechanism in Ge-Sb-Te based Chalcogenide Superlattices. *Sci. Rep.* **2016,** 6, 37325.
41. Sun, Z.; Pan, Y.; Zhou, J.; Sa, B.; Ahuja, R., Origin of p-type conductivity in layered nGeTe·mSb2Te3 chalcogenide semiconductors. *Phys. Rev. B* **2011,** 83, 113201.
42. Xu, M.; Zhang, W.; Mazzarello, R.; Wuttig, M., Disorder Control in Crystalline GeSb2Te4 using High Pressure. *Adv. Sci.* **2015,** 2, 1500117.
43. Jiang, Y.; Wang, Y.; Sagendorf, J.; West, D.; Kou, X.; Wei, X.; He, L.; Wang, K. L.; Zhang, S.; Zhang, Z., Direct atom-by-atom chemical identification of nanostructures and defects of topological insulators. *Nano Lett.* **2013,** 13, 2851-2856.
44. Saito, Y.; Fons, P.; Makino, K.; Mitrofanov, K. V.; Uesugi, F.; Takeguchi, M.; Kolobov, A. V.; Tominaga, J., Compositional tuning in sputter-grown highly-oriented Bi-Te films and their optical and electronic structures. *Nanoscale* **2017,** 9, 15115-15121.
45. Zou, Y.-C.; Chen, Z.-G.; Zhang, E.; Kong, F.; Lu, Y.; Wang, L.; Drennan, J.; Wang, Z.; Xiu, F.; Cho, K.; Zou, J., Atomic disorders in layer structured topological insulator SnBi2Te4 nanoplates. *Nano Res.* **2017,** 11, 696-706.
46. Zalden, P.; Siegert, K. S.; Rols, S.; Fischer, H. E.; Schlich, F.; Hu, T.; Wuttig, M., Specific Heat of (GeTe)x(Sb2Te3)1–xPhase-Change Materials: The Impact of Disorder and Anharmonicity. *Chem. Mater.* **2014,** 26, 2307-2312.
47. Siegert, K. S.; Lange, F. R.; Sittner, E. R.; Volker, H.; Schlockermann, C.; Siegrist, T.; Wuttig, M., Impact of vacancy ordering on thermal transport in crystalline phase-change materials. *Rep. Prog. Phys.* **2015,** 78, 013001.
48. Oliver, E.; Kornelius, N.; Nicola, P.; Friedemann, V., *Thermoelectric Bi2Te3 Nanomaterials*. WILEY-VCH: Weinheim, Germany, 2015.
49. Jiang, Y.; Zhang, X.; Wang, Y.; Wang, N.; West, D.; Zhang, S.; Zhang, Z., Vertical/Planar Growth and Surface Orientation of Bi2Te3 and Bi2Se3 Topological Insulator Nanoplates. *Nano lett.* **2015,** 15, 3147-3152.
50. Goedecker, S.; Teter, M.; Hutter, J., Separable dual-space Gaussian pseudopotentials. *Phys. Rev. B* **1996,** 54, 1703.
51. Perdew, J. P.; Burke, K.; Ernzerhof, M., Generalized Gradient Approximation Made Simple. *Phys. Rev. Lett.* **1996,** 77, 3865-3868.
52. Grimme, S., Semiempirical GGA-type density functional constructed with a long-range dispersion correction. *J. Comput. Chem.* **2006,** 27, 1787-1799.

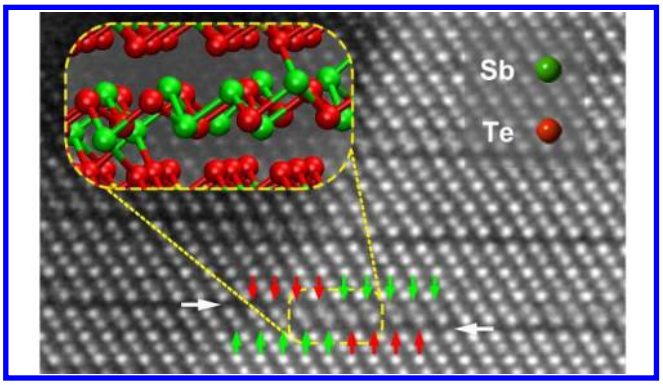
Sb
Te